Franck−Condon Simulation of the $S_1 \rightarrow S_0$ Spectrum of Phenol

S. Schumm, M. Gerhards,* and K. Kleinermanns

Heinrich-Heine Universität Düsseldorf, Institut für Physikalische Chemie und Elektrochemie I, D-40225 Düsseldorf, Germany

Received: January 13, 2000; In Final Form: August 17, 2000

In this paper, a Franck−Condon simulation of the $S_1 \rightarrow S_0$ transition of phenol is given including all normal modes. The geometries of phenol in its S_0 and S_1 states are obtained from CASSCF calculations. The calculated scaled harmonic frequencies are in good agreement with the experimental values. To calculate the Franck−Condon factors, Duschinsky rotations between the S_0 and S_1 states are taken into account. A very strong Duschinsky rotation is observed between modes 1 and 18a and modes 9b, 14, and the OH-bending vibration. To get good agreement between experimental and theoretical intensities, the calculated geometry of the S_1 state is fitted by reducing the C−O bond length and elongating the molecule along mode 6a. Thus, the most significant changes in geometry in the S_1 state can be deduced from the experimentally observed intensity pattern. The program developed to calculate the Franck−Condon factors is described and tested for the well-known spectrum of the benzene molecule. It is shown how the use of a hash table reduces storage space which is necessary for a multidimensional Franck−Condon analysis of large molecules.

I. Introduction

The relative intensities of vibronic bands in the electronic transitions of molecules is governed by the Franck−Condon (FC) principle.[1−2] Under the assumptions that the Born−Oppenheimer approximation[3] is valid and that the electronic transition moment varies only slowly with the internuclear distances, the probability of a vibronic transition is proportional to the square of the vibrational overlap integral between the initial and final states. These values are commonly known as Franck−Condon factors. To calculate the overlap integrals for polyatomic molecules, the normal modes of the final state have to be expressed in terms of the normal modes of the initial state. This problem has been qualitatively discussed by Duschinsky.[4] In this theoretical framework, the geometries and normal modes of a molecule in both electronic states are all that is needed to calculate the relative intensity distribution of a vibronic transition. Because of the development of methods such as the quantum consistent force field QCFF/PI of Warshel and Karplus[5] and ab initio techniques such as CIS[6] and CASSCF,[7] geometries and normal modes of small to medium size molecules in different electronic states can now be calculated routinely. On the basis of these methods, numerous applications of FC calculations have been presented in the literature.[8−23] Most of these studies just focus on the interpretation of experimentally known spectra. Because the geometry difference between two electronic states is a major factor that influences FC intensities, the simulation of vibronic spectra of polyatomic molecules can be regarded as a valuable test with respect to the quality of calculated geometries and as a starting point to obtain improved structures.

In this paper, a program is presented to calculate multidimensional Franck−Condon integrals and the application to the dispersed fluorescence spectrum of phenol ($S_1 \rightarrow S_0$ transition)[24] is given. As test case for our Franck−Condon program, the simulation of the direct absorption spectrum of benzene[25,26] has been chosen.

II. Calculation of Franck−Condon Integrals

Different methods[23,27−32] have been proposed to calculate multidimensional Franck−Condon integrals. We chose the recursion relations of Doctorov, Malkin, and Manko,[28] which are exact in the harmonic approximation, to calculate the FC integrals of the $S_1 \rightarrow S_0$ vibronic transitions of phenol. To our knowledge, Gruner et al.[8−11] were the first to apply this method to the spectra of larger molecules. Callis et al.[12,13] used the recursion relations to calculate the fluorescence spectra of indole. The derivation of the general expressions for the multidimensional FC integrals can be found either in the original work of Doctorov et al.[28] or in a recent paper of Berger et al.,[14] who analyzed the hot-band spectra of benzene and pyrazine. In this paper, only a brief overview of the equations involved in the calculation is given.

The harmonic vibrational eigenfunction of an *n*-atomic molecule can be specified by a set of $N = 3n - 6$ vibrational quantum numbers v_i: $|\bar{v}\rangle = |v_1, v_2, \ldots v_N\rangle$. The frequency associated with the normal coordinate q_i is denoted ω_i. The transformation between the normal coordinates of the two electronic states is given by[4,28,29]

$$q_i'' = \sum_k S_{ik} q_k' + d_i \qquad (1)$$

The vector **d** describes a translation in the 3*n*-dimensional coordinate space of the molecule, and the orthogonal matrix **S** defines a rotation in the normal coordinate space. The translation vector and the rotation matrix can be calculated from the normal coordinates and the equilibrium Cartesian configuration r_{eq} in the different electronic states:[8−10,29]

$$\mathbf{S} = (\mathbf{L}'')^{-1}\mathbf{L}' \qquad \mathbf{d} = (\mathbf{L}'')^{-1}\mathbf{M}^{1/2}(r_{eq}'' - r_{eq}') \qquad (2)$$

In eq 2, **L** is a matrix that contains the mass-weighted Cartesian normal coordinates as columns and **M** is a diagonal matrix of the atomic masses. It should be noted that a proper coordinate

10.1021/jp000187g CCC: $19.00
Published on Web 10/25/2000

TABLE 1: Rotational Constants of Phenol in Its Electronic Ground State and the First Excited State[c]

	S_0			S_1		
	A″	**B″**	**C″**	**A′**	**B′**	**C′**
experiment	5650.515[a]	2619.236[a]	1789.855[a]	5313.6[b]	2620.5[b]	1756.1[b]
CAS(8,7) cc-pVDZ	5659.3 (0.16)	2623.3 (0.16)	1792.4 (0.14)	5337.8 (0.46)	2572.0 (−1.85)	1735.7 (−1.16)
fitted CAS(8,7)				5294.9 (−0.35)	2624.9 (0.17)	1754.9 (0.06)

[a] See ref 38. [b] See ref 39. [c] All constants are given in MHz. The values in parentheses are the deviation from the experimental values in percent.

system must be chosen to describe the geometry of the initial and final electronic states.[33,34] According to Doctorov et al.,[28] the following matrixes are needed for the recursion relations:

$$\boldsymbol{\lambda}_{\omega} = \mathrm{diag}(\omega_1^{1/2}, \omega_2^{1/2}, ..., \omega_{3N}^{1/2}) \qquad \delta = \hbar^{-1/2}\boldsymbol{\lambda}_{\omega'}\mathbf{d}$$

$$\mathbf{J} = \boldsymbol{\lambda}_{\omega''}\mathbf{S}\boldsymbol{\lambda}_{\omega'}^{-1} \qquad \mathbf{Q} = (1 + \tilde{\mathbf{J}}\mathbf{J})^{-1} \qquad \mathbf{P} = \mathbf{J}\mathbf{Q}\tilde{\mathbf{J}}$$

$$\mathbf{R} = \mathbf{Q}\tilde{\mathbf{J}} \quad (3)$$

The tilde in eq 3 denotes the transpose matrix. Using the definition given in eqs 1−3, the recursion relations for emission and absorption are

$$\langle v_1'', ..., v_k'' + 1, ..., v_{3N-6}''|\vec{v}'\rangle = 2\sum_{i=1}^{3N-6} R_{ik}\left(\frac{v_i'}{v_k'' + 1}\right)^{1/2} \times \langle v_1'', ..., v_k'', ..., v_{3N-6}''|v_1', ..., v_i' - 1, ..., v_{3N-6}'\rangle + \sum_{l=1}^{3N-6} (2P - 1)_{kl}\left(\frac{v_l'}{v_k'' + 1}\right)^{1/2} \langle v_1'', ..., v_l'' - 1, ..., v_{3N-6}''|\vec{v}'\rangle - [(1 - P)\delta]_k\left(\frac{2}{v_k'' + 1}\right)^{1/2} \langle v_1'', ..., v_k'', ..., v_{3N-6}''|\vec{v}'\rangle \quad (4)$$

and

$$\langle \vec{v}''|v_1', ..., v_i' + 1, ..., v_{3N-6}'\rangle = 2\sum_{k=1}^{3N-6} R_{ik}\left(\frac{v_k''}{v_i' + 1}\right)^{1/2} \times \langle v_1'', ..., v_k'' - 1, ..., v_{3N-6}''|v_1', ..., v_i', ..., v_{3N-6}'\rangle + \sum_{j=1}^{3N-6} (2Q - 1)_{i,j}\left(\frac{v_j''}{v_i' + 1}\right)^{1/2} \langle \vec{v}''|v_1', ..., v_j' - 1, ..., v_{3N-6}'\rangle - (R\delta)_i\left(\frac{2}{v_i' + 1}\right)^{1/2} \langle \vec{v}''|v_1', ..., v_i', ..., v_{3N-6}'\rangle \quad (5)$$

Before eqs 4 and 5 can be used to calculate FC factors, the overlap integral of the electronic origin has to be calculated explicitly by

$$\langle \vec{0}''|\vec{0}'\rangle = 2^{3N-6/2}\left[\prod_{j=1}^{3N-6}\left(\frac{\omega_j''}{\omega_j'}\right)^{1/4}\right] \det(\mathbf{Q})^{1/2} \exp[-{}^1/_2\delta(1 - P)\delta] \quad (6)$$

Different algorithms have been proposed in the literature[8,14] to implement eqs 4 and 5 efficiently. Our own solution to this problem is explained in the appendix of this paper.

III. Geometries and Excitation Energies

CASSCF calculations have been performed for the S_0 and S_1 states of benzene and phenol using the Gaussian 94 and 98[35] programs. The CASSCF method is the best available method which can be applied to both the S_0 and S_1 states. By using the same method for the two electronic states, no artificial Duschinsky rotations of normal modes are obtained, which arise only from the application of different ab initio methods to describe the two states.

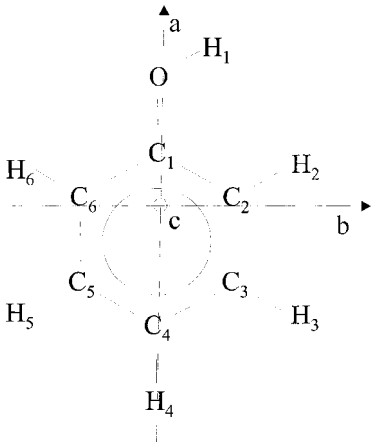

Figure 1. Labeling of the atoms and of the principal axes of inertia in phenol.

For the CASSCF calculations of benzene, an active space of the six π-orbitals of the aromatic ring has been chosen. The active space used for phenol was chosen by analogy to a previously published study[36] and consists of the six π-valence orbitals of the aromatic ring and the oxygen lone pair orbital which has π-symmetry. The active spaces of benzene and phenol are abbreviated as CAS(6,6) and CAS(8,7), respectively. For all calculations, the correlation consistent cc-pVDZ basis set[37] is used.

The rotational constants calculated for the S_0 and S_1 states of phenol are compared to the experimental values of Larsen[38] and Berden et al.[39] in Table 1. The geometry of the phenol molecule (cf. Figure 1) has been restricted to C_s symmetry. The calculated bond lengths and bond angles have been published in an earlier work.[36] The deviations between calculated and experimentally observed bond lengths and bond angles of the S_0 state are less than 0.01 Å and 1°, respectively. Only the C_1-O bond length and the C_1-O-H_1 bond angle (Figure 1) show slightly larger deviations (0.019 Å and 1.9°). Thus, the rotational constants obtained for the S_0 state are in very good agreement with the experimental values. Compared to the S_0 state, a larger deviation between the experimentally observed and calculated rotational constants is obtained for the S_1 state. This results mainly from the C−O bond length which is underestimated in the CASSCF calculations. A significant shortening of the C−O bond length of about 0.1 Å is predicted from high-resolution fluorescence excitation experiments, whereas only a small shortening (0.01 Å) is predicted by the CASSCF calculations. The C−O bond length is important in the discussion of the FC simulations. We demonstrate that the result of the simulation can be improved considerably by a small adjustment of the CASSCF geometry of the S_1 state (see section VI). The rotational constants of the fitted geometry are given in Table 1. These values show only small deviations from the experimentally obtained rotational constants.

TABLE 2: Differences between the Nomenclature of Bist et al. (Ref 40) and Varsányi (Ref 53)

Bist et al.	Varsányi	Bist et al.	Varsányi
11	10b	12	1
18b	15	15	18b
10b	11	7a	13
1	12		

TABLE 3: Vibrational Frequencies of Phenol in the S_0 State

mode	sym	expt[a]	CAS(8,7) cc-pVDZ	scaled
		In-Plane Vibrations[b]		
18b	b_2	403	430	401
6a	a_1	527	562	524
6b	b_2	619	664	619
12	a_1	823	870	811
1	a_1	999	1067	995
18a	a_1	1026	1092	1018
15	b_2	1070	1144	1067
9b[c]	b_2	1150	1184	
9a	a_1	1168	1251	1167
β(OH)	a_1	1176	1271	1185
7a	a_1	1261	1379	1286
3	b_2	1277	1462	1363
14[c]	b_2	1343	1358	
19b	b_2	1472	1597	1489
19a	a_1	1501	1633	1523
8b	a_1	1603[d]	1739	1622
8a	b_2	1610[d]	1757	1628
13	a_1	3027	3318	3033
7b	b_2	3049	3336	3049
2	a_1	3063	3348	3060
20b	b_2	3070	3362	3073
20a	a_1	3087	3370	3081
σ(OH)	a_1	3656	4162	
		Out-of-Plane Vibrations[e]		
11	b_1	244	249	240
τ(OH)	a_2	309	291	280
16a	a_2	409	436	420
16b	b_1	503	552	532
4	b_1	686	720	693
10b	b_1	751	774	745
10a	a_2	817	836	805
17b	b_1	881	898	865
17a	a_2	958[f]	975	939
5	b_1	973	1000	963

[a] See ref 24. [b] Scaling factors: σ(C−H) 7a−20a, 0.9141; others, 0.9326. [c] Kekulé modes (see text). [d] The order of modes 8a and 8b is reversed with respect to Bist et al. [e] Scaling factor: 0.9629. [f] Frequency taken from Green and Evans (cf. text).

The calculated excitation energy for the electronic origin of the $S_1 \rightarrow S_0$ transition of phenol is 37 076 cm^{-1}. This value includes zero point energy corrections (ZPE) using the unscaled harmonic frequencies of the CASSCF calculations. The calculated energy is in very good agreement with the experimental value of 36 349 cm^{-1}.[39]

IV. Vibrational Assignments

Numerous experimental[24,40−45] and theoretical[36,46−52] studies of the vibrational frequencies of phenol in its electronic ground state and first excited state have been published in the past. Our calculated scaled harmonic frequencies for phenol in the S_0 and S_1 states are compared in Tables 3 and 4 to the experimental frequencies published by Bist et al.[40,41] It has already been pointed out in the literature[24,50] that the nomenclature used by Bist et al. to assign the vibrational frequencies differs from the widely used nomenclature of Varsányi[53] for substituted benzenes. For historical reasons, we use the labeling of Bist et al. in Tables 3 and 4. The different labeling schemes of Varsányi and Bist et al. are given in Table 2.

TABLE 4: Vibrational Frequencies of Phenol in the S_1 State

mode	sym	expt[a]	new assignt	CAS(8,7) cc-pVDZ	scaled
		In-Plane Vibrations[b]			
18b	b_2	396		417	393
6a	a_1	475		506	477
6b	b_2	523		581	548
12	a_1	783		822	775
1	a_1	935		969	913
18a	a_1	958		1031	972
15	b_2	962		1013	955
9a[c]	a_1	975		1216	965
9b[c]	b_2	989		1234	979
β(OH)[c]	a_1	1005		1283	1018
3[c]	b_2	1131		1437	1140
7a	a_1	1273		1369	1291
19b	b_2	1478		1510	1423
19a	a_1	1498		1545	1456
8b	b_2			1675	1579
8a	a_1	1566		1699	1602
14	b_2	1180	1572	1867	1579[d]
13	a_1	3084		3345	3103
7b	b_2	3092		3355	3112
2	a_1			3371	3127
20b	b_2	3136		3380	3135
20a	a_1	3186		3393	3147
σ(OH)	a_1	3581		4156	
		Out-of-Plane Vibrations			
16a	a_2	187		271	
11	b_1	206	162	182	
4	b_1	358	465	371	
16b	b_1	441		472	
10a	a_2	580	615	540	
10b	b_1	615	580	492	
τ(OH)	a_2	635		285	
17b	b_1	700	726	616	
5	b_1	726	734	700	
17a	a_2	734	700	592	

[a] See ref 41. [b] Scaling factors: 9a−3, 0.7934; σ(CH): 7a−20a, 0.9276; 18b−15, 0.9427. [c] Vibrations with large in-plane CH bending components. [d] Estimated from the corresponding values of benzene (see text).

A few remarks must be made with respect to the vibrational frequencies of phenol in the S_0 state listed in Table 3. Bist et al. observed two bands at 1603 and 1610 cm^{-1}. In their interpretation, the band with the lower frequency was assigned to mode 8a. However, this is in contradiction to the experimental work of Green[44] and Varsányi.[53] Furthermore, Michalska et al.[49] pointed out that in ab initio calculations mode 8b always has the lower frequency. Because our calculations confirm this observation, we assign the band at 1603 cm^{-1} to mode 8b and the band at 1610 cm^{-1} to mode 8a (cf. Table 3). The frequency of mode 11 has been determined by Bist et al. to be 244 cm^{-1}. In a recent experimental study,[24] we were able to show that the correct frequency for this mode is 225 cm^{-1}, which is confirmed by our density-functional theory calculations[24] as well as an experimental study by Larsen and Nicolaisen.[54] In contrast to Green,[41] Evans,[43] and Keresztury et al.,[46] who determined a frequency of 958 cm^{-1} for mode 17a, a frequency of 995 cm^{-1} is given by Bist et al. for this mode. Because our calculations indicate that mode 17a should have a lower frequency than mode 5 at 973 cm^{-1}, we used the value of 958 cm^{-1} for mode 17a in Table 3. All frequencies listed in Table 3 are scaled except modes 9b and 14. These Kekulé modes correspond to a deformation of the molecule toward localized double bonds. It was shown for benzene that highly correlated methods such as CCSD(T) in combination with large basis sets are necessary to

TABLE 5: Duschinsky Matrix of the In-Plane Modes of Phenol[a]

	S_1															
S_0	18b	6a	6b	12	1	15	18a	9a	9b	β(OH)	7a	3	19b	19a	8b	8a	14
18b	0.989																
6a		0.999															
6b	0.008		0.991														
12				0.974	0.013												
1					0.314		0.674										
18a				0.02	0.652		0.304							0.016			
15						0.925				0.023			0.029				0.011
9b						0.022			0.282	0.190					0.008		0.464
9a								0.982									
β(OH)									0.647	0.272					0.006		0.063
14									0.061	0.499	0.018						0.407
7a											0.967					0.007	0.013
3												0.985					0.008
19b						0.035							0.948				
19a					0.014									0.963		0.009	
8b															0.975		0.019
8a																0.977	

[a] Given are the squares of the matrix elements.

TABLE 6: Duschinsky Matrix of the Out-of-Plane Modes of Phenol[a]

	S_1									
S_0	11	16a	τ(OH)	16b	4	10a	10b	17a	17b	5
11	0.970		0.024							
16a	0.022	0.091	0.822	0.028		0.033				
τ(OH)		0.901	0.097							
16b			0.028	0.886		0.015	0.059			
4				0.014	0.825	0.107	0.040			
10a				0.068	0.096	0.115	0.562	0.047	0.070	0.041
10b			0.021		0.046	0.683	0.220	0.019		
17a					0.028	0.014	0.112	0.089	0.594	0.162
17b						0.032		0.835	0.072	0.057
5									0.253	0.736

[a] Given are the squares of the matrix elements.

calculate the frequencies for the Kekulé modes correctly.[55] In the case of our CASSCF calculations, the unscaled frequencies are quite close to the experimental frequencies because of a compensation of errors resulting from the neglect of dynamical correlation and the choice of a double-ζ basis set.

Concerning the vibrations of the S_1 state (see Table 4), a few differences with respect to the original assignment of Bist et al.[40,41] have to be discussed. It has been shown experimentally[56] as well as in several theoretical studies[57−62] on different aromatic molecules that the frequency of the Kekulé mode 14 is larger in the S_1 state than in the S_0 state. A detailed explanation of this behavior has been given by Shaik et al.[58,59] However, Bist et al. assigned mode 14 in the S_1 state to a band at a lower frequency (1180 cm^{-1}) than that in the S_0 state (1343 cm^{-1}). Because we assume that the frequency of the S_0 state is correct, the assignment for the S_1 state must be wrong. Concerning the vibrational frequencies of benzene in the S_1 state,[63] we were able to show that both the CASSCF and the CIS method tend to overestimate the frequency of mode 14 in the S_1 state. Using the results for benzene, we can estimate a frequency of 1580 cm^{-1} for this vibration in phenol. Bist et al. observed two weak bands at 1572 and 1598 cm^{-1} in the UV-absorption spectrum of phenol. They assigned these transitions to the second overtone of mode 6b and to the combination band $7a_0^1\ \tau(OH)_1^1$, respectively. One of these bands should be assigned to mode 14.

For symmetry reasons, Bist et al.[40,41] were not able to observe the out-of-plane modes as fundamental transitions in the UV-absorption spectrum of phenol. Their assignment of these modes is based on observed overtones and hot bands and must be viewed with some caution. In a recent experimental study,[24] we examined the four most intense hot bands in the UV spectrum of phenol using dispersed fluorescence spectroscopy (DF) and spectral hole burning (SHB). We were able to show that the interpretation given by Bist et al. for these bands is wrong. On the basis of these results, we determined the frequencies of modes 11 and 4 to be 162 and 465 cm^{-1}, respectively. Unfortunately, the calculated frequencies for the out-of-plane modes are not accurate enough to give definite results for the assignment of the other out-of-plane modes. In Table 4, we give an alternative assignment for the out-of-plane vibrations that is based on the calculated Duschinsky matrix (see below).

TABLE 7: Duschinsky Matrix of the OH- and CH-Stretching Vibrations[a]

	S_1					
S_0	13	7b	2	20b	20	σ(OH)
13	0.998					
7b		0.858	0.069	0.066		
2		0.051	0.921	0.021		
20b		0.073		0.900	0.022	
20		0.018		0.012	0.965	
σ(OH)						1.00

[a] Given are the squares of the matrix elements.

V. Duschinsky Rotations in Phenol

The Duschinsky matrix **S** has been calculated from the normal modes of the S_0 and S_1 states according to eq 2. The results are summarized in Tables 5−7 as a list of the square of the matrix elements S_{ij}. We give only elements larger than 0.01. The sum over the elements in each column and row should be close to unity. On the basis of the calculated structure of the Duschinsky

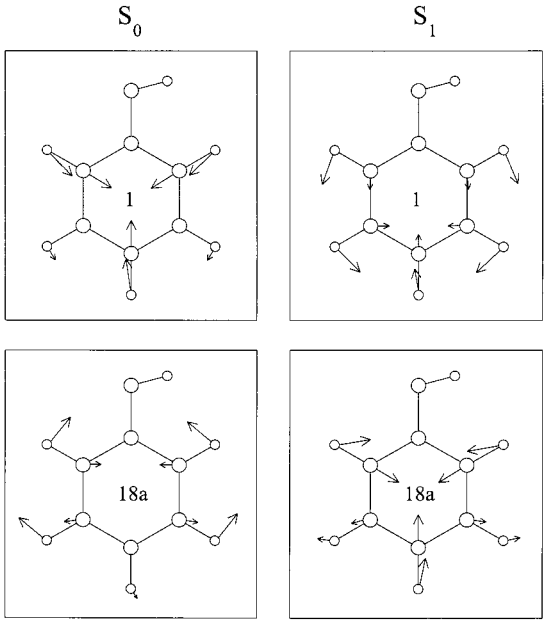

Figure 2. Duschinsky rotation of modes 1 and 18a.

matrix, the vibrations can be divided into three different groups that do not interact with each other. By symmetry arguments, it is apparent that the out-of-plane modes (Table 7) do not interact with the in-plane modes and that the Duschinsky matrix should be block-diagonal. In addition to this obvious separation, it was found that the CH-stretching vibrations (Table 6) do not interact with the other in-plane vibrations. For the in-plane vibrations, two very strong Duschinsky rotations are found in our study (Table 5). The first one is between mode 1 and mode 18a. From Table 5 and Figure 2, it is apparent that the vibration at 935 cm^{-1} in the S_1 state (assigned to mode 1 by Bist et al.) is more closely related to mode 18a in the ground state than to mode 1 and vice versa.

The Duschinsky rotation between the OH-bending vibration and modes 9b and 14 is illustrated in Figure 3. It should be noted that in the S_0 state modes 9b and 14 both have CH-bending and CC-stretching character, whereas in the S_1 state mode 9b is a nearly pure CH-bending vibration and mode 14 is a CC-stretching vibration with a small component of the OH-bending mode (β(OH), cf. Figure 3). Mode 9b in the S_1 state is dominated by a linear combination of mode 9b and β(OH) of the S_0 state. Because of this linear combination, the OH-bending component nearly cancels out in the S_1 state. This Duschinsky effect is typical for aromatic molecules and is associated with the fact that mode 14 has a higher frequency in the S_1 state than in the S_0 state. In contrast to theoretical studies[57−62] on other aromatic systems in which normally only two modes are reported to couple in this way, we observe a coupling of three modes.

The out-of-plane modes show much more mode scrambling than the in-plane modes. Because the quality of the calculated frequencies for these modes is different in the S_0 and S_1 states, some of the observed coupling might be artificial. The alternative assignment given in Table 6 for these modes is based on the assumption that a mode of the S_1 state should be labeled in the same way as the mode in the S_0 state that it most resembles.

VI. Franck−Condon Simulations

To test our program as well as the quality of the geometries and normal modes, we first performed a FC simulation of the $S_1(B_{2u}) \leftarrow S_0(A_{1g})$ transition of benzene using the geometries

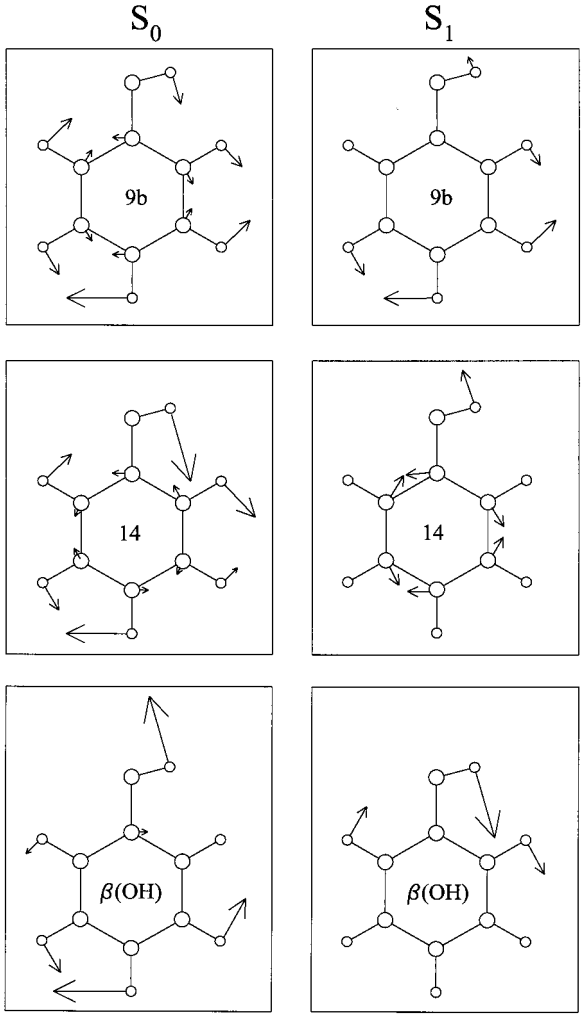

Figure 3. Duschinsky rotation of the Kekulé modes. For better visualization, the size of elongation vectors has been scaled for each normal mode. The scaling factor is the same for all elongations of one normal mode.

and normal modes obtained from the CASSCF calculations for the S_0 and S_1 states. The progression of mode 1 taken from a direct absorption spectrum of jet-cooled benzene[25] and the simulations are shown in Figure 4. The simulated and experimentally observed relative intensities are listed in Table 8. Because mode 1 corresponds to a symmetric extension of the aromatic ring ("ring breathing"), an accurate description of the change in the CC bond lengths due to electronic excitation is essential for the FC simulation of this vibronic transition. The simulation based on the CASSCF geometries reproduces the experimental intensity pattern very well. The result of the FC simulation supports our assumption that the CASSCF method leads to a correct description of the change in the CC bond length upon electronic excitation in aromatic systems.

Figure 5 compares the FC simulation of phenol to a dispersed fluorescence (DF) spectrum[24] that was obtained by exciting the electronic origin of the $S_1 \leftarrow S_0$ transition. The inset in Figure 5b displays the simulation that was obtained using the CASSCF geometries for both the S_0 and S_1 states without a fit. From the prominent bands that can be observed in the experimental fluorescence spectrum in the region up to 1800 cm^{-1} relative to the electronic origin, the mode 6a was missing in the simulation. Bist et al.[41] already noted that the change in the rotational constants upon electronic excitation can be interpreted as a deformation of the molecule in the S_1 state along mode 6a or mode 8a. The best agreement between the FC simulation

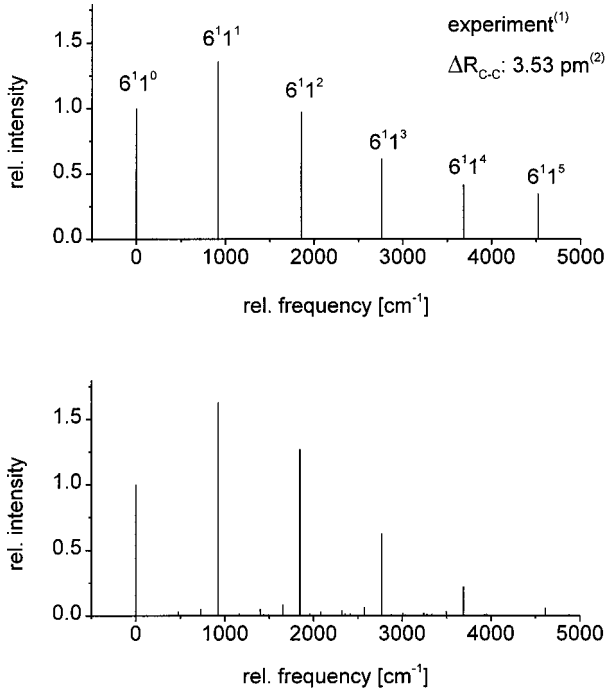

Figure 4. Franck−Condon simulation of the $S_1(^1B_{2u}) \leftarrow S_0(^1A_{1g})$ transition in benzene: (1) ref 25 and (2) ref 26.

TABLE 8: Experimentally Observed and Simulated Intensities of the Direct Absorption Spectrum of Benzene[a] and the Dispersed Fluorescence Spectrum of Phenol by Exciting the Origin of the $S_1 \leftarrow S_0$ Transition[b,c]

transition (assignt)	expt intensity	simulated intensity	transition (assignment)	expt intensity	simulated intensity
			Benzene		
$6a^1 1^0$	1.00	1.00	$6a^1 1^3$	0.62	0.63
$6a^1 1^1$	1.36	1.63	$6a^1 1^4$	0.42	0.22
$6a^1 1^2$	0.98	1.27	$6a^1 1^5$	0.35	0.06
			Phenol		
11^2	0.04	0.02	$6a^2$	0.07	0.10
6a	0.81	0.58	7a	0.52	0.66
6b	0.04	0.02	6a+12	0.15	0.25
$16a^2$	0.19	0.09	4^2	0.04	0.05
12	1.00	1.00	$10a^2$	0.11	0.06
1	0.57	1.64	12^2	0.08	0.24
$16b^2$	0.40	0.02	6a+7a	0.12	0.16
18a	0.33	0.16			

[a] See ref 25. [b] See ref 24. [c] The large difference between the calculated and experimental values of the 1, $16b^2$, and 18a modes of phenol results from a Fermi resonance (see text). The intensity of the phenol spectrum is normalized to the 12 mode because the intensity of the electronic origin is falsified by stray light.

and experiment was obtained by first shortening the C−O bond to 1.335 Å and then elongating the geometry along mode 6a (total elongation 0.04 Å). Because mode 6a shows no Duschinsky rotation with other modes (Table 7), the intensity of the remaining modes is not influenced by this procedure. During the fitting procedure, which was performed manually, only those changes in the geometry were considered that led to an improvement in the rotational constants for the S_1 state. The rotational constants for the fitted geometry are listed in Table 1. The corresponding Franck−Condon simulation is displayed in Figure 5b. The simulated and experimentally observed relative intensities are listed in Table 8. In the spectral region marked as A in Figure 5, three strong bands assigned as modes 1, $16b^2$, and 18a can be observed in the experiment, whereas only modes 1 and 18a have a large intensity in the simulation. The reason for this is a Fermi resonance between mode 1 and mode $16b^2$

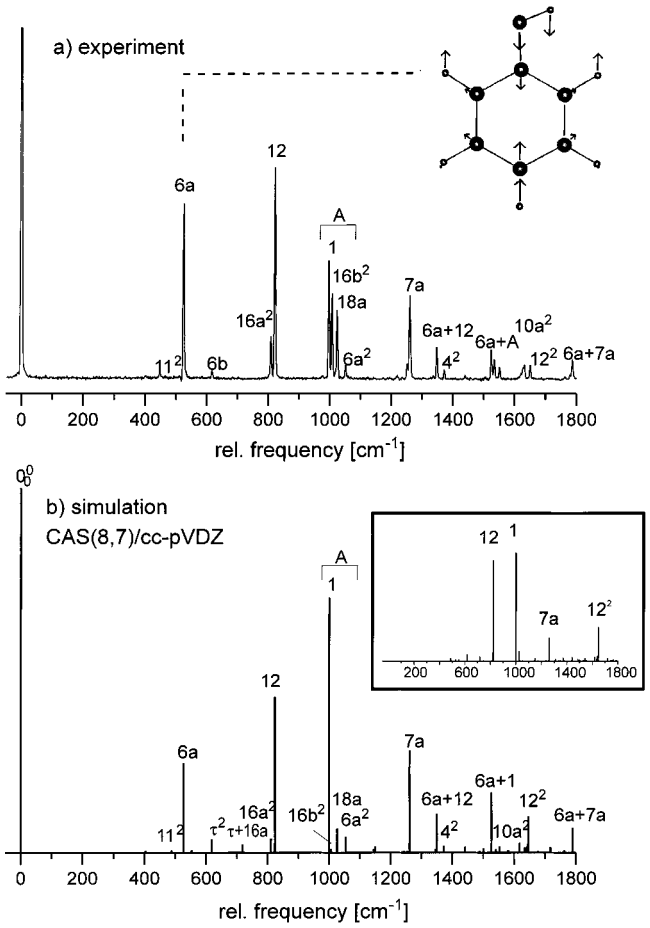

Figure 5. Franck−Condon simulation of the $S_1(^1A') \rightarrow S_0(^1A')$ transition in phenol. The difference in the intensity pattern between experimental and simulated spectra in region A (modes 1, $16b^2$, and 18a) is a result of the Fermi resonance between modes 1 and $16b^2$ (ref 45) which cannot be taken into account on the basis of a harmonic oscillator approximation. The inset of Figure 5b displays the simulated spectrum without fitting mode 6a and the C−O bond length.

that has been postulated by Wilson et al.[45] Because effects such as Fermi resonances are not taken into account in the harmonic approximation used in our simulation, this behavior is not reproduced correctly in our calculation. However, the integrated intensity of the three modes is close to the experimental value. All other main features of the experimental spectrum are reproduced in our simulation, which underlines the validity of the assumptions made with regard to the CASSCF geometry of the aromatic ring.

Our comparison between the dispersed fluorescence spectrum of phenol and its Franck−Condon simulation shows very good agreement between the experimental and the calculated intensity pattern. According to our Franck−Condon fit, the CC bond length increases by 0.027 Å (on average), whereas the C−O bond length decreases by 0.023 Å on $S_1 \leftarrow S_0$ excitation. In our future work, we will perform multidimensional Franck−Condon simulations of aromatic molecules and clusters to get information about geometry changes after electronic excitations.

Acknowledgment. The authors thank the Deutsche Forschungsgemeinschaft for financial support. We acknowledge the granted computer time from the Universitätsrechenzentrum Düsseldorf and the Regionales Rechenzentrum der Universität zu Köln.

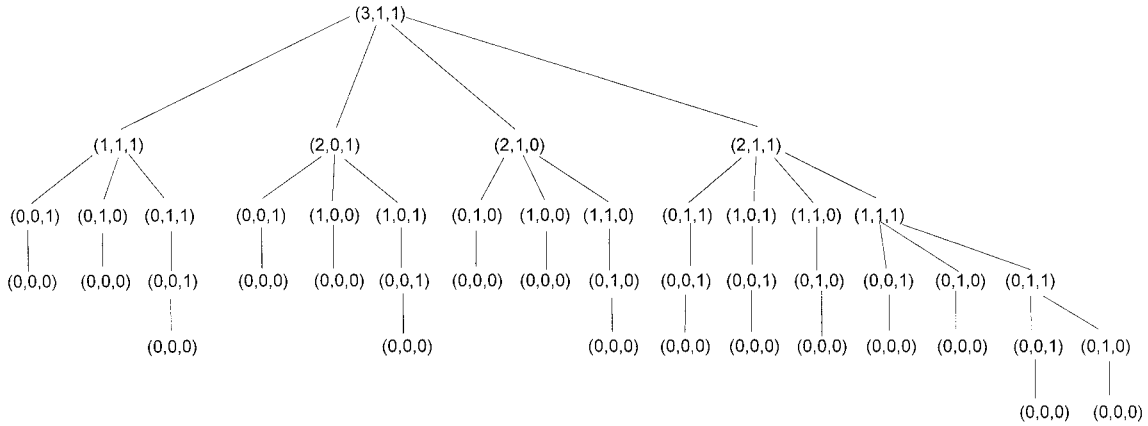

Figure 6. Recursion tree for the calculation of the overlap integral $\langle 000 \mid 311 \rangle$.

Appendix

The recursion relations 4 and 5 can be used in two different ways. The most general way is to calculate hot-band spectra. At higher temperatures, absorption spectra can originate from different vibrational levels of the electronic ground state. In this case, the main challenge is to determine the quantum numbers of all possible vibronic transitions that fall into a given energy region. An algorithm that used a backtracking procedure has been applied by Berger et al.[14,64] to calculate the hot-band spectra of benzene and pyrazine. Many modern spectroscopic techniques use molecular beam expansion and laser excitation to prepare the molecular system under investigation in a certain well-defined initial vibronic state. Our program was designed with these techniques in mind, and we consider only transitions that originate from one specific vibronic state.

For simplicity, we restrict the following discussion to those transitions that originate from the vibrational ground state of the initial electronic state. The procedure outlined below can easily be extended to spectra that originate from a vibrationally excited molecule. To explain the use of the recursion relations, we choose a molecule with three vibrational degrees of freedom. If we use the convention that the recursion is always applied to the mode with the highest number of vibrational quanta, then all the integrals in the recursion tree in Figure 6 are needed in order to calculate the overlap integral $\langle \bar{0}|3,1,1\rangle$ which has been taken as an example. From Figure 6, it becomes apparent that in a sequential execution of the recursion relation some of the integrals need to be calculated several times. To avoid this and to evaluate eqs 4 and 5 efficiently, two problems must be solved: the integrals must be generated in a specific order and each integral must be stored in a way that allows it to be accessed in an arbitrary order. Storage of integrals in a multidimensional array that uses the set of N vibrational quantum numbers as an index is possible only for small systems. Gruner and Brumer[8] have demonstrated how the storage problem can be solved using a binary tree. In this paper, we present an alternative method that employs a hash table[65] to store the integrals.

An elegant way to solve the problem of generating and storing the integrals can be found by interpreting the quantum numbers for a molecule with N vibrational degrees of freedom as a N-figured polyadic number to the base B. The number $B - 1$ denotes the maximum number of quanta allowed in each vibrational mode. With $B = 3$, the state vector 10200_3 (the index indicates the base) corresponds to $1 \times B^4 + 2 \times B^2 = 99_{10}$ in the decimal system. Thus by simply counting the decimal numbers up from zero all indices can be generated in the desired order. For a molecule like phenol with $N = 33$ and $B = 6$, a total of 2.8×10^{26} different state vectors can be generated in this way. This number can be reduced drastically by imposing the following restrictions on the simulation:

1. Only vibrations up to a given maximum energy E_{max} are considered.

2. Only a given number of modes can be excited simultaneously.

3. The total number of vibrational quanta in all modes is restricted.

4. The maximum number of vibrational quanta in one mode is $B - 1$.

Criterion 4 is already included in the definition of the polyadic system used. The other restrictions are checked during the calculation. For an efficient execution, it is also necessary to ignore nonplausible groups of numbers. If restrictions 1−3 are not satisfied, the digits in at least one place of the polyadic number have to be carried over to generate an acceptable state vector. This is achieved by setting the zeros in the lower valued places to $B - 1$. This is illustrated in the following example:

$0000001_3 \rightarrow E < E_{max}$: calculate overlap

$+1 = 0000002_3 \rightarrow E < E_{max}$: calculate overlap

... .

$+1 = 0022010_3 \rightarrow E > E_{max}$:
set new index to 0022012_3

$+1 = 0022020_3 \rightarrow E$ still larger than E_{max}:
set new index to 0022222_3

$+1 = 0100000_3 \rightarrow E < E_{max}$: calculate overlap

For every state vector that satisfies conditions 1−3, a numerical value for the respective FC integral is calculated and stored.

For a small problem, it would be feasible to convert the polyadic number that represents the state vector into the decimal system and use it as the index in a linear array. For larger problems, the size of the array would very soon reach the capability of standard PCs or workstations. Because of restrictions 1−3, only a small number of the elements in such an array are actually needed. A standard algorithm to tackle such a problem is hashing.

In its simplest form, a hash table is just a linear array that contains in each of its elements the information to be stored (the overlap integral), a hash key, and a flag that indicates if an element is occupied. The hash algorithm consists of a transformation that assigns a table index to every hash key as well

as a collision treatment. Because the number of possible keys is much greater than the number of elements in the table, an unambiguous key transformation is not possible. The collision treatment generates a new index whenever the transformation does not reach the desired result (e.g., the indexed element is already occupied in the writing process). We use a standard collision treatment that has been proposed by Wirth:[65]

$$h = (h_0 + i^2) \text{ modulo } size \qquad (7)$$

Here, h_0 is the original index, i is the number of collisions, and *size* is the number of elements in the hash table. For efficient execution, the key transformation and the collision treatment must be fast and the number of the collisions should be small. Because the number of collisions increases with the occupancy of the hash table, it is mandatory to use a table with more entries than integrals to be stored.

An efficient key transformation should map the possible keys uniformly on the existing indices to avoid collisions. To transform the polyadic number into a decimal number would be efficient but feasible only for small problems. Starting from the left, we are free to identify the digits in the polyadic number with the vibrational frequencies in ascending order. Because of energy restriction 1, we find low frequency modes excited in more state vectors than modes with higher frequencies. In the case of phenol, a key transformation that interprets the first six digits in a completely polyadic manner and generates a reduced polyadic number for the remaining numbers by deleting all zeros was found to be effective. In this way, the state vector

$$000201000200101201200 1_3 = 818974045_{10}$$

would be reduced to

$$212112012001_3 = 1368469_{10}$$

References and Notes

(1) Franck, J. *Trans. Faraday Soc.* **1925**, *21*, 536.
(2) Condon, E. U. *Phys. Rev.* **1926**, *28*, 1182; **1928**, *32*, 858.
(3) Born, M.; Oppenheimer, R. *Ann. Phys.* **1927**, *84*, 457.
(4) Duschinsky, F. *Acta Physicochim. URSS* **1937**, *7*, 551.
(5) Warshel, A.; Karplus, M. *J. Am. Chem. Soc.* **1972**, *94*, 5612.
(6) Foresman, J. B.; Head-Gordon, M.; Pople, J. A.; Frisch, M. J. *J. Phys. Chem.* **1992**, *96*, 135.
(7) Roos, B. O. The Complete Active Space Self-Consistent Field Method and its Applications in Electronic Structure Calculations. In *Ab initio Methods in Quantum Chemistry*; Lawles, K. P., Ed.; John Wiley & Sons Ltd: Chichester, 1987; Vol. 2.
(8) Gruner, D.; Brumer, P. *Chem. Phys. Lett.* **1987**, *138*, 310.
(9) Gruner, D.; Brumer, P. *J. Chem. Phys.* **1990**, *94*, 2862.
(10) Gruner, D.; Nguyen, A.; Brumer, P. *J. Chem. Phys.* **1994**, *101*, 10366.
(11) Dods, J.; Gruner, D.; Brumer, P. *Chem. Phys. Lett.* **1996**, *261*, 612.
(12) Vivian, J. T.; Callis, P. R. *Chem. Phys. Lett.* **1994**, *229*, 153.
(13) Callis, P. R.; Vivian, J. T.; Slater, L. S. *Chem. Phys. Lett.* **1995**, *244*, 53.
(14) Berger, R.; Fischer, C.; Klessinger, M. *J. Phys. Chem. A* **1998**, *102*, 7157.
(15) Zgierski, M. Z.; Zerbetto, F. *J. Chem. Phys.* **1993**, *99*, 3721.
(16) Negri, F.; Zgierski, M. Z. *J. Chem. Phys.* **1993**, *99*, 4318.
(17) Buma, W. J.; Zerbetto, F. *J. Chem. Phys.* **1995**, *103*, 10492.
(18) Orlandi, G.; Palmieri, P.; Tarroni, R.; Zerbetto, F.; Zgierski, M. Z. *J. Chem. Phys.* **1994**, *100*, 2458.
(19) Mebel, A. M.; Chen, Y.-T.; Lin, S.-H. *J. Chem. Phys.* **1996**, *105*, 9007.
(20) Mebel, A. M.; Chen, Y.-T.; Lin, S.-H. *Chem. Phys. Lett.* **1996**, *258*, 53.
(21) Mebel, A. M.; Chen, Y.-T.; Lin, S.-H. *Chem. Phys. Lett.* **1997**, *275*, 19.
(22) Hemley, R. J.; Leopold, D. G.; Vaida, V.; Karplus, M. *J. Chem. Phys.* **1985**, *82*, 5379.
(23) Faulkner, T. R.; Richardson, F. S. *J. Chem. Phys.* **1979**, *70*, 12011.
(24) Roth, W.; Imhof, P.; Gerhards, M.; Schumm, S.; Kleinermanns, K. *Chem. Phys.* **2000**, *252*, 247.
(25) Hiraya, A.; Shobatake, K. *J. Chem. Phys.* **1991**, *94*, 7700.
(26) Neusser, H. J.; Schlag, E. W. *Angew. Chem.* **1992**, *104*, 269.
(27) Doktorov, E. V.; Malkin, I. A.; Man'ko, V. I. *J. Mol. Spectrosc.* **1975**, *56*, 1.
(28) Doktorov, E. V.; Malkin, I. A.; Man'ko, V. I. *J. Mol. Spectrosc.* **1977**, *64*, 302.
(29) Sharp, T. E.; Rosenstock, H. M. *J. Chem. Phys.* **1964**, *41*, 3453.
(30) Kupka, H.; Cribb, P. H. *J. Chem. Phys.* **1986**, *85*, 1303.
(31) Chen, K.; Pei, C. *Chem. Phys. Lett.* **1990**, *165*, 523.
(32) Baranov, V. I.; Zelent'sov, D. Y. *J. Mol. Struct.* **1992**, *272*, 283.
(33) Pickett, H. M.; Strauss, H. L. *J. Am. Chem. Soc.* **1970**, *92*, 7281.
(34) Louck, J. D.; Galbraith, H. W. *Rev. Mod. Phys.* **1976**, *48*, 69.
(35) Frisch, M. J.; Trucks, G. W.; Schlegel, H. B.; Gill, P. M. W.; Johnson, B. G.; Robb, M. A.; Cheeseman, J. R.; Keith, T.; Petersson, G. A.; Montgomery, J. A.; Raghavachari, K.; Al-Laham, M. A.; Zakrzewski, V. G.; Ortiz, J. V.; Foresman, J. B.; Cioslowski, J.; Stefanov, B. B.; Nanayakkara, A.; Challacombe, M.; Peng, C. Y.; Ayala, P. Y.; Chen, W.; Wong, M. W.; Andres, J. L.; Replogle, E. S.; Gomperts, R.; Martin, R. L.; Fox, D. J.; Binkley, J. S.; Defrees, D. J.; Baker, J.; Stewart, J. P.; Head-Gordon, M.; Gonzalez, C.; Pople, J. A. *Gaussian 94*, revision E.2; Gaussian, Inc.: Pittsburgh, PA, 1995.
(36) Schumm, S.; Gerhards, M.; Roth, W.; Gier, H.; Kleinermanns, K. *Chem. Phys. Lett.* **1996**, *263*, 126.
(37) Dunning, T. H. *J. Chem. Phys.* **1989**, *90*, 1007.
(38) Larsen, N. *J. Mol. Struct.* **1979**, *51*, 175.
(39) Berden, G.; Meerts, W. L.; Schmitt, M.; Kleinermanns, K. *J. Chem. Phys.* **1996**, *104*, 972.
(40) Bist, H. D.; Brand, J. C. D.; Williams, D. R. *J. Mol. Spectrosc.* **1967**, *24*, 413.
(41) Bist, H. D.; Brand, J. C. D.; Williams, D. R. *J. Mol. Spectrosc.* **1967**, *24*, 402.
(42) Bist, H. D.; Brand, J. C. D.; Williams, D. R. *J. Mol. Spectrosc.* **1966**, *21*, 76.
(43) Evans, J. C. *Spectrochim. Acta* **1960**, *16*, 1382.
(44) Green, H. S. *J. Chem. Soc.* **1961**, 2236.
(45) Wilson, H. W.; MacNamee, R. W.; Durig, J. R. *J. Raman Spectrosc.* **1981**, *11*, 252.
(46) Keresztury, G.; Billes, F.; Kubinyi, M.; Sundius, T. *J. Phys. Chem. A* **1998**, *102*, 1371.
(47) Lampert, H.; Mikenda, W.; Karpfen, A. *J. Phys. Chem. A* **1997**, *101*, 2254.
(48) Brand, J. C. D.; Califano, S.; Williams, D. R. *J. Mol. Spectrosc.* **1968**, *26*, 398.
(49) Michalska, D.; Bienko, D. C.; Abkowicz-Bienko, A. J.; Latajka, Z. *J. Phys. Chem.* **1996**, *100*, 17786.
(50) Krauss, M.; Jensen, J. O.; Hameka, H. F. *J. Phys. Chem.* **1994**, *98*, 9955.
(51) Smeyers, Y. G.; Hernández-Laguna, A. *Int. J. Quantum Chem.* **1982**, *22*, 681.
(52) Venuti, E.; Marconi, G. *J. Mol. Struct.* **1992**, *266*, 235.
(53) Varsányi, G. *The Assignment of Vibrational Spectra of 700 Benzene Derivatives*; Academic Press: Budapest, 1973.
(54) Larsen, N. W.; Nicolaisen, F. M. *J. Mol. Struct.* **1974**, *22*, 29.
(55) Martin, J. M. L.; Taylor, P. R.; Lee, T. J. *Chem. Phys. Lett.* **1997**, *275*, 414.
(56) Metz, F.; Robey, M. J.; Schlag, E. W. *Chem. Phys. Lett.* **1977**, *51*, 8.
(57) Swiderek, P.; Hohlneicher, G. *J. Chem. Phys.* **1993**, *98*, 974.
(58) Shaik, S.; Shurki, A.; Danovick, D.; Hiberty, P. C. *J. Am. Chem. Soc.* **1996**, *118*, 666.
(59) Shaik, S.; Shurki, A.; Danovick, D.; Hiberty, P. C. *THEOCHEM* **1997**, 398.
(60) Zilberg, S.; Kendler, S.; Haas, Y. *J. Phys. Chem.* **1996**, *100*, 10869.
(61) Zilberg, S.; Haas, Y. *J. Chem. Phys.* **1995**, *103*, 20.
(62) Zilberg, S.; Haas, Y.; Shaik, S. *J. Phys. Chem.* **1995**, *99*, 16558.
(63) Schumm, S.; Gerhards, M. Unpublished results.
(64) Berger, R.; Klessinger, M. *J. Comput. Chem.* **1997**, *18*, 1312.
(65) Wirth, N. *Algorithmen und Datenstrukturen*; B. G. Teubner Publisher: Stuttgart, 1983.